Biochemical and Biophysical Research Communications 458 (2015) 515–519

Contents lists available at ScienceDirect

Biochemical and Biophysical Research Communications

journal homepage: www.elsevier.com/locate/ybbrc

Effects of an ATP analogue, adenosine 5′-[α-thio]-triphosphate, on F_1-ATPase rotary catalysis, torque generation, and inhibited intermediated formation

Ayako Yukawa [a], Rikiya Watanabe [a, b, c, *], Hiroyuki Noji [a, b, *]

[a] Department of Applied Chemistry, Graduate School of Engineering, The University of Tokyo, Tokyo 113-8656, Japan
[b] JST, CREST, Tokyo 113-8656, Japan
[c] JST, PRESTO, Tokyo 113-8656, Japan

ARTICLE INFO

Article history:
Received 24 January 2015
Available online 12 February 2015

Keywords:
F_1-ATPase
F_oF_1-ATP synthase
Single-molecule analysis
Molecular motor
ATP analogue

ABSTRACT

F_1-ATPase (F_1), an important rotary motor protein, converts the chemical energy of ATP hydrolysis into mechanical energy using rotary motion with extremely high efficiency. The energy-conversion mechanism for this molecular motor has been extensively clarified by previous studies, which indicate that the interactions between the catalytic residues and the β- and γ-phosphates of ATP are indispensable for efficient catalysis and torque generation. However, the role of α-phosphate is largely unknown. In this study, we observed the rotation of F_1 fuelled with an ATP analogue, adenosine 5′-[α-thio]-triphosphate (ATPαS), in which the oxygen has been substituted with a sulfur ion to perturb the α-phosphate/F_1 interactions. In doing so, we have revealed that ATPαS does not appear to have any impact on the kinetic properties of the motor or on torque generation compared to ATP. On the other hand, F_1 was observed to lapse into the ADP-inhibited intermediate states when in the presence of ATPαS more severely than in the presence of ATP, suggesting that the α-phosphate group of ATP contributes to the avoidance of ADP-inhibited intermediate formation.

1. Introduction

F_1-ATPase (F_1), the water-soluble portion of the F_oF_1-ATP synthase complex, is an ATP-driven rotary molecular motor [1,2,3]. Bacterial F_1 is composed of $\alpha_3\beta_3\gamma\delta\varepsilon$ subunits; however, only the $\alpha_3\beta_3\gamma$ subcomplex is required for motor function [4]. The $\alpha_3\beta_3$ subunits of this minimal motor form the stator ring and the γ subunit acts as the rotary shaft [5,6,7]. Further, the three catalytic sites, which mainly reside on the β subunits at the α-β interfaces [5,6,7] (Fig. 1A), hydrolyze ATP in a highly cooperative manner to drive the unidirectional rotation of the γ subunit. Through this mechanism, F_1 converts chemical energy to mechanical work in an extremely efficient manner. For example, in thermophilic *Bacillus* PS3 (TF_1) and *Escherichia coli* (EF_1), the levels of rotary torque generated by F_1 have been estimated to be 40 pN nm [8,9] and 20–74 pN nm [10,11,12], respectively, which are comparable to the energy released through simple ATP hydrolysis in these species.

Elucidation of the full reaction scheme of F_1 has been accomplished primarily using single-molecule techniques focusing on the mechanism of TF_1 [8,13–17]. According to current literature, the elementary step size of the rotation is 120°, and each step is coupled with a single turnover of ATP hydrolysis [8]. This 120° step can be further separated into 80° and 40° substeps [13], which are triggered by ATP binding/ADP release and ATP cleavage/P_i release, respectively [14,15,18]. Notably, the angular positions of F_1 before the 80° and 40° substeps are referred to as the binding and catalytic angles, respectively.

Recently, we investigated the role of individual ATP moieties (i.e., base, and triphosphates) during F_1 rotary catalysis [19–21]. The role of the base moiety of ATP was determined using a base-free nucleotide (ribose triphosphate, RTP). Notably, even though the binding rate of RTP to the motor was retarded 2.2×10^5 fold, lacking the base did not hinder the rotation of F_1, which still generated torque similar to that observed during normal ATP-

Abbreviations: F_1, F_1-ATPase; TF_1, F_1-ATPase from thermophilic *Bacillus* PS3; EF_1, F_1-ATPase from *Escherichia coli*; ATPαS, adenosine 5′-[α-thio]-triphosphate; ATPγS, adenosine 5′-[γ-thio]-triphosphate.

* Corresponding authors. Department of Applied Chemistry, Graduate School of Engineering, The University of Tokyo, Tokyo 113-8656, Japan. Fax: +81 3 5841 1872.
E-mail addresses: wrikiya@nojilab.t.u-tokyo.ac.jp (R. Watanabe), hnoji@appchem.t.u-tokyo.ac.jp (H. Noji).

http://dx.doi.org/10.1016/j.bbrc.2015.01.146
0006-291X/

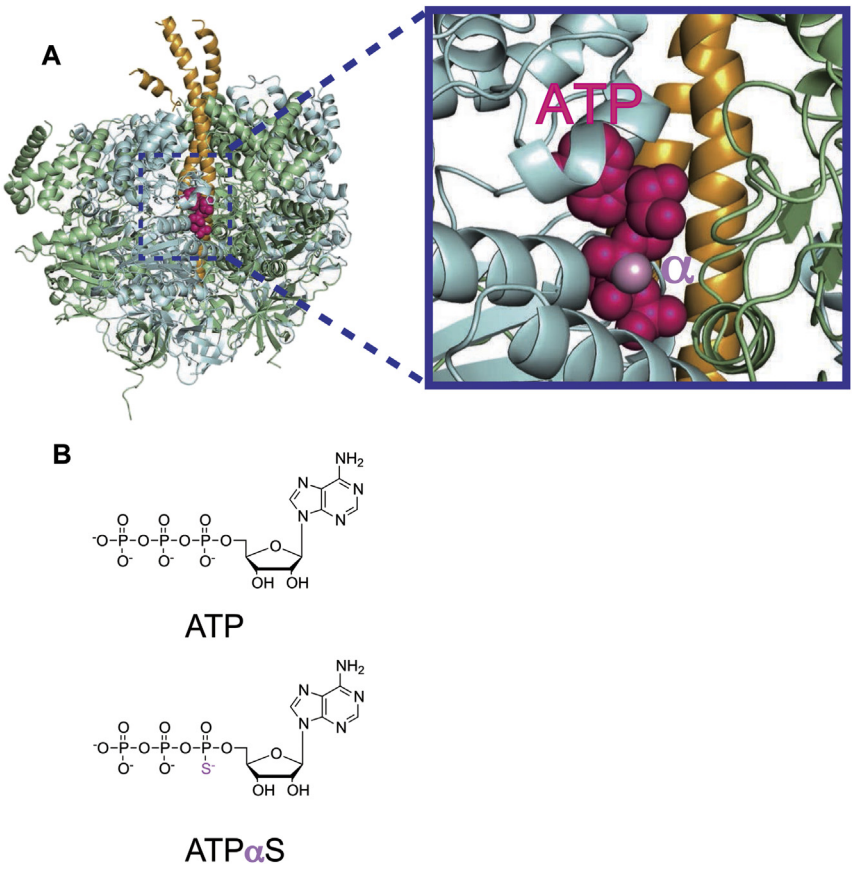

Fig. 1. Position of ATPαS bound to the catalytic site of F_1 and chemical structures of ATP and ATPαS. A, Crystal structure of mitochondrial F_1 viewed from the side, β_{DP}/α_{DP} catalytic interface (PDB code: 1BMF). The α, β, and γ subunits are shown in *pearlgreen*, *pearlblue*, and *pearlyellow*, respectively. AMP-PNP bound to the catalytic site is shown as a pink space-filling model and the oxygen bound to the α-phosphate is highlighted in *pearlpink*. B, Chemical structures of ATP and ATPαS. The oxygen ion bound to the α-phosphate is substituted with a sulfate ion, shown in *pearlpink*. (For interpretation of the references to color in this figure caption, the reader is referred to the web version of this article.)

driven rotation [19]. Thus, these findings indicate that the base moiety of ATP is likely required for efficient catalysis, but not for torque generation. On the other hand, the role of the triphosphate moiety appears to play a larger function during torque generation. To study this, we used F_1 mutated at the catalytically critical residues of the p-loop lysine and the arginine finger, which are known to directly interact with the β- and γ-phosphates of ATP [20–22]. When the arginine finger was substituted with lysine or the natural amino acid 2,7-diaminoheptanoic acid (Lyk), which still retain the electrostatic interactions with the β- and γ-phosphates of ATP, we observed a 500-fold decrease in catalytic activity. However, these mutants appeared to generate almost the same amount of rotary torque compared to the 5′-[γ-thio]-triphosphate (ATPγS), which specifically perturbs the γ-phosphate, but still retains the electrostatic interactions [14]. In contrast, when the residues are substituted with alanine, which completely eliminates the electrostatic interactions with the ATP molecule, the catalytic activity was extremely slow and torque generation was diminished to only half of the normal levels [21]. Thus, it appears that the β- and γ-phosphates of ATP are indispensable for efficient catalysis and torque generation.

Notably, the role of the α-phosphate, the first phosphate of the ATP triphosphate moiety, during F_1 rotary catalysis is largely unknown. In the present study, we have investigated the function of this α-phosphate using commercially available adenosine 5′-[α-thio]-triphosphate (ATPαS) (Fig. 1B), which specifically perturbs the α-phosphate-mediated interactions between ATP and the rotary motor. The details of ligand binding/release related to the α-phosphate were resolved using a single molecule rotational assay, and the role of the α-phosphate during the complex rotary catalysis of the F_1 motor was identified. Taken together, these data indicate that interaction with the α-phosphate is not crucial for efficient catalysis, but likely contributes to avoid formation of ADP-inhibited intermediates.

2. Materials and methods

2.1. Purity assessment of the ATPαS solution

Purity of the ATPαS solution (Jena Bioscience, Germany) was assessed using HPLC with an anion-exchange column. Nucleotides (1 mM ATP or 1 mM ATPαS) were applied to a POROS HQ 20 micron 10 mmD/100 mmL column (Lifetechnologies, USA) equilibrated with eluent A (50 mM MOPS-KOH buffer (pH 7.0)) and eluted with an appropriate eluent A and eluent B (50 mM MOPS-KOH, 500 mM K_2SO_4 (pH 7.0)) program (A/B = −isocratic at 100/0 for 2 min, linear gradient to 0/100 in 6 min, then isocratic at 0/100 for 4 min). We monitored the absorbance of each elution volume at 260 nm (A_{260}) (Fig. S1a). To assess the ATP contamination in the ATPαS buffer, we analyzed the elution profiles of three independent samples with known levels of contamination: 1 mM ATPαS without ATP (Buffer A), 1 mM ATPαS with 15 μM ATP (Buffer B), 1 mM ATPαS with 50 μM ATP (Buffer C), and 1 mM ATPαS with 150 μM ATP (Buffer D) (Fig. S1b). A calibration curve was established using these buffers by calculating the area values for each ATP-peak (Fig. S1c), and this

curve was then used to determine the ATP contamination present in the ATPαS solution.

2.2. Rotation assay

TF_1 was isolated as previously reported [23], and a flow chamber was prepared for the rotation assay (<20 μL) according to the methods established by Yasuda et al. [13]. F_1 was immobilized onto a Nickel-Nitrilotriacetic Acid (Ni-NTA)-modified glass surface via polyhistidine-tags (His-tags). Analysis of the rotational Michaelis–Menten enzyme kinetics was conducted using 60 nm colloidal gold as a non-frictional rotation marker [13,24]. The rotations were observed using a high-speed camera (FASTCAM-1024PCI, Photron, Japan). Further, magnetic beads (0.2–0.4 μm, Seradyn, USA) were used to measure the level of torque, rotary potential, and inhibition. We used a phase-contrast microscope (IX-70; Olympus, Japan) with a 100 × objective. Images were recorded at 3000 frames per second (fps) for the Michaelis–Menten, torque, and rotary potential measurements and 30 fps for the inhibition analysis. All experiments were conducted at pH 7.

3. Results

3.1. Rotary motion of F_1 in the presence of ATPαS

Commercial ATPαS was used for the rotation assay without further purification. ATP contamination in the ATPαS sample was below the detection limit (i.e., present at <0.1%) of our analysis (see Fig. S1). Using colloidal gold ($\phi = 60$ nm), the rotation of wild-type F_1 was observed at various ATPαS concentrations, ranging from 1 μM to 1 mM (Fig. 2A). Notably, the viscous friction exerted by the colloidal gold on the γ subunit has been shown to be very low, allowing full-speed rotation of F_1 [13,24], implying that any change in rotation is due to the presence of ATPαS rather than ATP. The rotational values obtained for ATPαS appeared to obey a simple Michaelis–Menten curve (Fig. 2B), similar to a previous report [13], with a maximum rotation rate (V_{max}) of 100 s^{-1} and a Michaelis constant (K_m) of 91 μM. The binding rate constant (k_{on}) of ATPαS, defined as $k_{on} = 3 \times V_{max}/K_m$ [13], was found to be 3.3×10^6 M^{-1} s^{-1}. Notably, this binding rate is 6.7 times lower than that of ATP (2.2×10^7 M^{-1} s^{-1}, Table 1). While the $k_{on}^{ATP\alpha S}/k_{on}^{ATP}$ is only 15%, these data suggest that substitution with ATPαS still allows F_1 rotation. Notably, the contribution of possible ATP contamination (<0.1%) to this binding is negligible.

Furthermore, the measured V_{max} for each concentration of ATPαS was also evaluated in terms of the individual reaction steps comprising ATP hydrolysis (e.g., hydrolysis and product release) [13]. In the presence of 1 mM ATPαS, F_1 was observed to rotate with discrete 120° steps. The distribution of the dwell-time before each 120° step exhibited a typical convex curve indicative of a sequential reaction, whereby $y = C \cdot (\exp(-k_1 \cdot t) - \exp(-k_2 \cdot t))$ with k_1 and k_2 values of 7.8×10^2 s^{-1} and 8.5×10^2 s^{-1}, respectively (Fig. 2C). Following our previous observation that the slower step corresponds to hydrolysis while the faster step represents P_i release [25], these values (7.8×10^2 s^{-1} and 8.5×10^2 s^{-1}) represent the rate constants for ATPαS hydrolysis (k_{hyd}) and P_i release (k_{off}^{Pi}), respectively. Notably, these values are almost equal to those observed for ATP (summarized in Table 1), indicating that the kinetic effects of substituting a sulfate ion for the oxygen bound to the α-phosphate of ATP was minor, unlike ATPγS [14].

3.2. Measurement of torque and rotary potential

To compare the torque produced during ATPαS- and ATP- driven rotation of F_1, we measured the angular velocities of these rotations

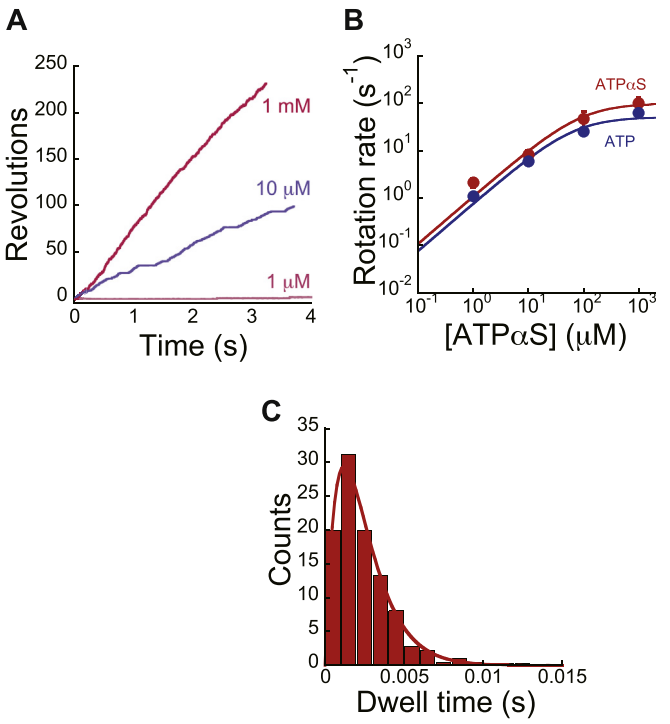

Fig. 2. Rotational time courses and kinetic analyses. A, Examples of the wild-type F_1 rotational time courses observed at 1 mM (*brightpink*), 10 μM (*pearlpurple*), and 1 μM ATPαS (*pearlpink*) using colloidal gold. B, Rate of wild-type F_1 rotation at various ATPαS (*red*) and ATP (*blue*) concentrations determined using colloidal gold. Error bars were calculated using at least five different molecules. The data was fitted with the Michaelis–Menten equation, $v = V_{max} \times [\text{ATP}\alpha\text{S or ATP}]/(K_m + [\text{ATP}\alpha\text{S or ATP}])$, while the binding rate constant (k_{on}) of ATPαS or ATP was determined from $3 \times V_{max}/K_m$ [13]. C, Histograms of the dwelling times between steps at an ATPαS concentration of 1 mM. Images were recorded at 3000 fps. The solid line represents a fitted curve using two exponents, whereby $y = C \times (\exp(-k_{hyd} \times t) - \exp(-k_{off}^{Pi} \times t))$, taking into consideration the two rate-limiting reactions involved: ATPαS hydrolysis and phosphate release. These kinetic values (k_{on}, k_{hyd}, and k_{off}^{Pi}) are summarized in Table 1. (For interpretation of the references to color in this figure caption, the reader is referred to the web version of this article.)

by conducing buffer-exchange experiments, whereby ATPαS buffer was exchanged for ATP buffer. To this end, magnetic beads ($\phi = 0.2$–0.4 μm) were used as the rotation probe, and the angular velocity ratio of the ATPαS- to ATP- driven rotation ($\omega_{ATP\alpha S}/\omega_{ATP}$) was determined. Fig. 3A represents the typical time courses of 1 μM ATPαS and 200 nM ATP, in which each slope value for the green lines corresponds to the angular velocity ($\omega_{ATP\alpha S}$ or ω_{ATP}, respectively). Data was collected for nine molecules of each nucleotide. Further, $\omega_{ATP\alpha S}/\omega_{ATP}$ was 0.95 ± 0.21 (mean ± S.D.) (Fig. 3B), indicating that the rotational torque driven by ATPαS (44 ± 4 pN nm) was comparable to that driven by ATP (43 ± 3 pN nm) (Table 1).

Next, in order to investigate the effects of ATPαS on the stability of the F_1 complex, we determined the torsional stiffness. Notably, the apparent torsional stiffness is dependent on at least two elastic components: the elasticity of the γ subunit and the rotary potential between the αβ stator ring and the γ subunit [23]. The former is typically the dominant factor in determining torsion stiffness of the wild-type F_1 in the presence of ATP. However, when the rotary

Table 1
Kinetic parameters, torque, and stiffness.

Nucleotide	k_{on} (M^{-1} s^{-1})	k_{hyd} (s^{-1})	k_{off}^{Pi}(s^{-1})	N (pN nm)	κ (pN nm)
ATP	2.2×10^7	6.7×10^2	2.0×10^3	43 ± 3	73.9
ATPαS	3.3×10^6	7.8×10^2	8.5×10^2	44 ± 4	63.1

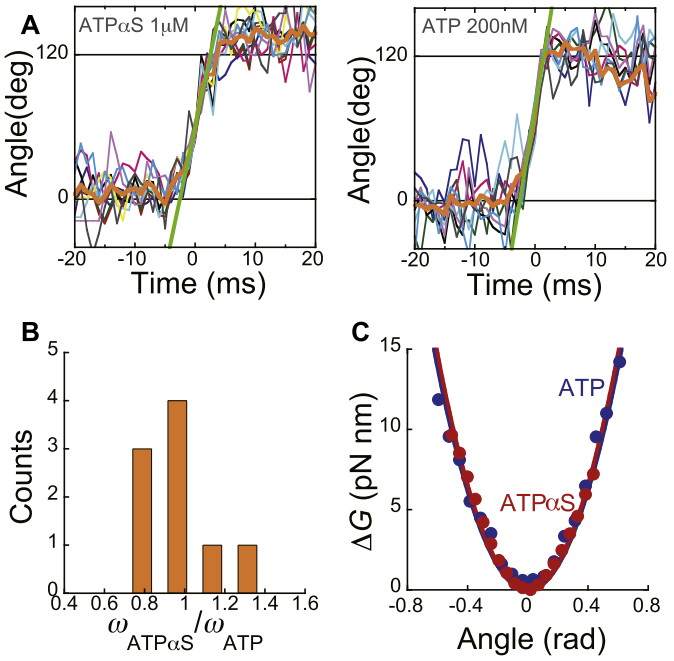

Fig. 3. Torque and rotary potential. A, Time courses of the stepping rotation observed for wild-type F_1 in the presence of 1 μM ATPαS (*left*) and 200 nM ATP (*right*). Buffer was exchanged from 1 μM ATPαS to 200 nM ATP. The thin lines show eight successive steps along with their averages (*thick orange lines*). The thick green lines show the linear fittings of the average steps between 40° and 80°. B, Histograms of the angular velocity ratios ($\omega_{ATP\alpha S}/\omega_{ATP}$). The mean value of the ratios is 0.95, indicating that the calculated rotary torque for ATPαS and ATP are 44 ± 4 pN nm and 43 ± 3 pN nm, respectively. C, Rotary potential observed during the catalytic pause. The probability densities of angular position during the pause were analyzed for nine molecules for both ATPαS (*red*) and ATP (*blue*) and transformed into the rotary potential according to the Boltzmann's law. These rotary potentials were then used to calculate stiffness (κ) using the harmonic function, $\Delta G = (1/2)\kappa\theta^2$. The stiffness was determined to be 63 pN nm and 74 pN nm for ATPαS and ATP, respectively. The torque and rotary potential values are summarized in Table 1. (For interpretation of the references to color in this figure caption, the reader is referred to the web version of this article.)

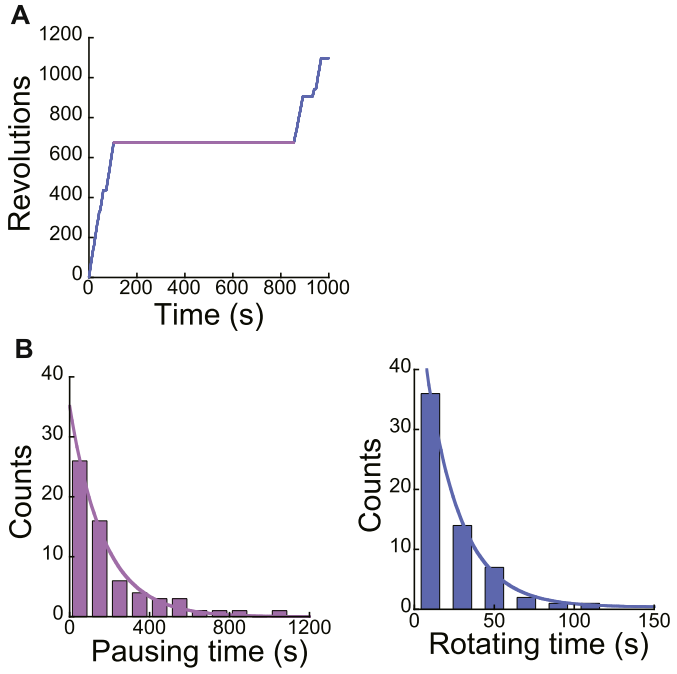

Fig. 4. Analysis of ADP-inhibited intermediate formation (long pauses). A, Representative rotational time course containing a long pause (*pearlpink*). B, Distribution of pause times before resuming the rotations (*pearlpink*) and the rotation times prior to lapsing into the long pause (*pearlblue*). Each solid line shows the fitted single-exponential decay function with a time constant of 171 s and 22 s, respectively. (For interpretation of the references to color in this figure caption, the reader is referred to the web version of this article.)

potential is largely weakened, the torsional stiffness has also been shown to be significantly lowered and appears to correlate well with the rotary torque [19–21]. Thus, the apparent stiffness can be used as a barometer for how stably the αβ stator ring holds the γ subunit. In this study, the probability distribution of γ-subunit orientation during the binding-waiting pauses was measured at 3000 fps, and the rotary potentials were determined from this probability distribution according to the Boltzmann law (Fig. 3C). The torsion stiffness (κ) was then estimated by fitting the calculated rotary potentials to the harmonic function, $\Delta G = 1/2 \times \kappa \times \theta^2$. In the presence of ATPαS, the torsional stiffness of F_1 was 63 pN nm during the binding-waiting pauses. These values are comparable to the torsional stiffness determined in the presence of ATP (74 pN nm, Fig. 3C, Table 1), which is similar to that previously reported (79 pN nm) [21]. Thus, while the stiffness and the calculated torque appeared to be correlated, similar to a previous report [21], the effect of sulfate substitution on these levels was minor.

3.3. Formation of ADP-inhibited intermediates

F_1 has previously been shown to form severely inhibited ADP-bound intermediate states during hydrolysis [26–29]. To determine the role of the α-phosphate in this inhibited state, we compared the duration of time spent in the rotating ($\tau_{rotating}$) or inhibited states ($\tau_{pausing}$) in the presence of ATPαS or ATP (Fig. 4A, Table 2). Fig. 4B shows the histograms of the time spent in each phase in terms of ATPαS. Notably, compared to ATP, ATPαS appeared to elongate the duration of time spent in the inhibited state by 5 fold, while the time spent in the rotating state was unchanged. Therefore, we conclude that disruption of the interactions between the α-phosphate of ATP and F_1 results in an increased likelihood of ADP-inhibited intermediate formation.

4. Discussion

Our experiments have shown that substituting ATPαS for ATP does not have a prominent impact on the kinetic parameters of F_1. Further, the differences in the rate constants for nucleotide binding (k_{on}), hydrolysis (k_{hyd}), and P_i release (k_{off}^{Pi}) between ATPαS and ATP was minor compared with other ATP analogues, such as ATPγS and base-substituted analogues [14,19]. In addition, it appears that the substitution of a sulfate ion for the oxygen bound to the α-phosphate of ATP was irrelevant for rotary-torque generation and did not affect the stability of the complex, even though these two values have been shown to be positively correlated with each other in previous studies [21]. Therefore, we conclude that the α-phosphate group of ATP does not directly participate in the catalytic processes utilized during F_1 motor function and torque generation.

It should be noted that the activation rate from the ADP-inhibited intermediate state ($k_{act} = 1/\tau_{pausing}$) using ATPαS is approximately five times slower than that observed using ATP, while the inactivation rate ($k_{inact} = 1/\tau_{rotating}$) for ATPαS was almost the same as that for ATP. Notably, previous studies have revealed that the activation rate from the ADP-inhibited state is suppressed by the addition of ADP [27] while the inactivation rate is suppressed by addition of P_i [27], suggesting that ADP release and improper P_i release likely triggers the activation and inactivation from ADP-inhibited state, respectively [30]. One possible interpretation of

Table 2
Duration of the rotation state (τ_{pause}) and the inhibited state ($\tau_{rotation}$).

Nucleotide	τ_{pause} (s)	$\tau_{rotation}$ (s)
ATP	32	22
ATPαS	171	22

the asymmetric effects of ATPαS we observed on ADP inhibition is that ATPαS may specifically perturb the α-phosphate, disrupting ADP release, but has no effect on γ-phosphate, which is known to be involved in P_i release following hydrolysis. Thus, specific changes in the interactions between α-phosphate and F_1 likely result in the isolated effect on the activation rate from the ADP-inhibited intermediate state. To verify this, future work should focus on simultaneously visualizing F_1 rotary motion and fluorescent-labeled ATPαS/ADPαS bound to the catalytic site of the ATPase.

Furthermore, this study demonstrates the potential use of the ATP analogues, ATPαS, which has allowed us to investigate the role of the triphosphate moiety of ATP in greater detail. To date, a large portion of the research concerning F_1, as well as other molecular motors, has focused on the changes observed following protein mutation; however, this study highlights the prospective utilization of nucleotide or ligand modifications using high resolution techniques. The use of this ATP analogue has helped to further differentiate between the functional roles of the three phosphate groups during F_1 rotary catalysis in addition to advancing our knowledge concerning the general mechanism of ATP-driven molecular motors.

Conflict of interest

There are no conflicts of interest to declare.

Acknowledgments

This work was supported in part by Grants-in-Aid for Scientific Research (30540108 to R.W. and 18074005 to H.N.) from the Ministry of Education, Culture, Sports, Science and Technology, Japan. We thank all the members of the Noji laboratory for valuable discussion.

Appendix A. Supplementary data

Supplementary data related to this article can be found at http://dx.doi.org/10.1016/j.bbrc.2015.01.146

References

[1] J. Weber, Structural biology: toward the ATP synthase mechanism, Nat. Chem. Biol. 6 (2010) 794–795.
[2] W. Junge, H. Sielaff, S. Engelbrecht, Torque generation and elastic power transmission in the rotary F_oF_1-ATPase, Nature 459 (2009) 364–370.
[3] M. Yoshida, E. Muneyuki, T. Hisabori, ATP synthase–a marvellous rotary engine of the cell, Nat. Rev. Mol. Cell. Biol. 2 (2001) 669–677.
[4] H. Noji, R. Yasuda, M. Yoshida, K. Kinosita Jr., Direct observation of the rotation of F_1-ATPase, Nature 386 (1997) 299–302.
[5] J.P. Abrahams, A.G. Leslie, R. Lutter, J.E. Walker, Structure at 2.8 Å resolution of F_1-ATPase from bovine heart mitochondria, Nature 370 (1994) 621–628.
[6] V. Kabaleeswaran, N. Puri, J.E. Walker, A.G. Leslie, D.M. Mueller, Novel features of the rotary catalytic mechanism revealed in the structure of yeast F_1 ATPase, EMBO J. 25 (2006) 5433–5442.
[7] G. Cingolani, T.M. Duncan, Structure of the ATP synthase catalytic complex (F_1) from Escherichia coli in an autoinhibited conformation, Nat. Struct. Mol. Biol. 18 (2011) 701–707.
[8] R. Yasuda, H. Noji, K. Kinosita Jr., M. Yoshida, F_1-ATPase is a highly efficient molecular motor that rotates with discrete 120 degree steps, Cell 93 (1998) 1117–1124.
[9] K. Hayashi, H. Ueno, R. Iino, H. Noji, Fluctuation theorem applied to F_1-ATPase, Phys. Rev. Lett. 104 (2010) 218103.
[10] D. Spetzler, R. Ishmukhametov, T. Hornung, L.J. Day, J. Martin, W.D. Frasch, Single molecule measurements of F_1-ATPase reveal an interdependence between the power stroke and the dwell duration, Biochemistry 48 (2009) 7979–7985.
[11] D.A. Cherepanov, W. Junge, Viscoelastic dynamics of actin filaments coupled to rotary F-ATPase: curvature as an indicator of the torque, Biophys. J. 81 (2001) 1234–1244.
[12] T. Bilyard, M. Nakanishi-Matsui, B.C. Steel, T. Pilizota, A.L. Nord, H. Hosokawa, M. Futai, R.M. Berry, High-resolution single-molecule characterization of the enzymatic states in Escherichia coli F_1-ATPase, Philos. Trans. R. Soc. Lond B Biol. Sci. 368 (2013) 20120023.
[13] R. Yasuda, H. Noji, M. Yoshida, K. Kinosita Jr., H. Itoh, Resolution of distinct rotational substeps by submillisecond kinetic analysis of F_1-ATPase, Nature 410 (2001) 898–904.
[14] K. Shimabukuro, R. Yasuda, E. Muneyuki, K.Y. Hara, K. Kinosita Jr., M. Yoshida, Catalysis and rotation of F_1 motor: cleavage of ATP at the catalytic site occurs in 1 ms before 40 degree substep rotation, Proc. Natl. Acad. Sci. U S A 100 (2003) 14731–14736.
[15] K. Adachi, K. Oiwa, T. Nishizaka, S. Furuike, H. Noji, H. Itoh, M. Yoshida, K. Kinosita Jr., Coupling of rotation and catalysis in F_1-ATPase revealed by single-molecule imaging and manipulation, Cell 130 (2007) 309–321.
[16] T. Ariga, E. Muneyuki, M. Yoshida, F_1-ATPase rotates by an asymmetric, sequential mechanism using all three catalytic subunits, Nat. Struct. Mol. Biol. 14 (2007) 841–846.
[17] R. Watanabe, R. Iino, H. Noji, Phosphate release in F_1-ATPase catalytic cycle follows ADP release, Nat. Chem. Biol. 6 (2010) 814–820.
[18] J.L. Martin, R. Ishmukhametov, T. Hornung, Z. Ahmad, W.D. Frasch, Anatomy of F_1-ATPase powered rotation, Proc. Natl. Acad. Sci. U S A 111 (2014) 3715–3720.
[19] H.C. Arai, A. Yukawa, R.J. Iwatate, M. Kamiya, R. Watanabe, Y. Urano, H. Noji, Torque generation mechanism of F_1-ATPase upon NTP binding, Biophys. J. 107 (2014) 156–164.
[20] Y. Komoriya, T. Ariga, R. Iino, H. Imamura, D. Okuno, H. Noji, Principal role of the arginine finger in rotary catalysis of F_1-ATPase, J. Biol. Chem. 287 (2012) 15134–15142.
[21] R. Watanabe, Y. Matsukage, A. Yukawa, K.V. Tabata, H. Noji, Robustness of the rotary catalysis mechanism of F_1-ATPase, J. Biol. Chem. 289 (2014) 19331–19340.
[22] A. Yukawa, R. Iino, R. Watanabe, S. Hayashi, H. Noji, Key chemical factors of arginine finger catalysis of F_1-ATPase clarified by an unnatural amino acid mutation, Biochemistry (2015) 472–480.
[23] D. Okuno, R. Iino, H. Noji, Stiffness of gamma subunit of F_1-ATPase, Eur. Biophys. J. 39 (2010) 1589–1596.
[24] R. Watanabe, Y. Minagawa, H. Noji, Thermodynamic analysis of F_1-ATPase rotary catalysis using high-speed imaging, Protein Sci. 23 (2014) 1773–1779.
[25] R. Watanabe, K. Hayashi, H. Ueno, H. Noji, Catalysis-enhancement via rotary fluctuation of F_1-ATPase, Biophys. J. 105 (2013) 2385–2391.
[26] Y. Hirono-Hara, H. Noji, M. Nishiura, E. Muneyuki, K.Y. Hara, R. Yasuda, K. Kinosita Jr., M. Yoshida, Pause and rotation of F_1-ATPase during catalysis, Proc. Natl. Acad. Sci. U S A 98 (2001) 13649–13654.
[27] N. Mitome, S. Ono, T. Suzuki, K. Shimabukuro, E. Muneyuki, M. Yoshida, The presence of phosphate at a catalytic site suppresses the formation of the MgADP-inhibited form of F_1-ATPase,, Eur. J. Biochem. 269 (2002) 53–60.
[28] Y.M. Milgrom, P.D. Boyer, The Adp that binds tightly to nucleotide-depleted mitochondrial F_1-ATPase and inhibits catalysis is bound at a catalytic site, Biochim Biophys Acta 1020 (1990) 43–48.
[29] D.J. Hyndman, Y.M. Milgrom, E.A. Bramhall, R.L. Cross, Nucleotide-binding sites on Escherichia coli F_1-ATPase. Specificity of noncatalytic sites and inhibition at catalytic sites by MgADP, J. Biol. Chem. 269 (1994) 28871–28877.
[30] R. Watanabe, H. Noji, Timing of inorganic phosphate release modulates the catalytic activity of ATP-driven rotary motor protein, Nat. Commun. 5 (2014) 3486.